The impact of thermal insulation on cooling energy consumption and optimal insulation thickness for underground tunnel

Yijiang Wang [a]*, Chaochao Wang [a], Shang Gao [a], Xiaofeng Zheng [b]*, Jo Darkwa [b]

[a] State key laboratory for Geomechanics and Deep Underground Engineering, School of Mechanics and Civil Engineering, China University of Mining and Technology, Xuzhou 221116, China

[b] Faculty of Engineering, University of Nottingham, University Park, Nottingham NG7 2RD, UK

Corresponding authors: Y. Wang (yjwang@cumt.edu.cn), X. Zheng(xiaofeng.zheng@nottingham.ac.uk)

Abstract: The provision of mechanical cooling in deep mines comes with a significant energy cost as a significant amount of heat transfers from surrounding rock to the airflow. Thermal insulation can be applied to reduce such heat transfer, thereby cutting down the cooling load. In this study, the impact of thermal insulation on reducing the heat flux through the rock was analytically investigated. The optimal insulation thickness, life cycle saving and the payback period were also evaluated by using the life cycle cost method as the economic benefit is heavily dependent on the insulation thickness. Results show that heat flux between tunnel and airflow can be significantly reduced by the use of thermal insulation, but the reduction varies with the tunnel and insulation conditions. The total cost associated with using the thermal insulation firstly decreases and then increases when the insulation thickness increases, implying an optimal insulation thickness. Nonetheless, both the optimal insulation thickness and maximum life cycle saving can be increased by a rising rock temperature, eventually leading to a reduced payback period.

Keywords: thermal insulation; cooling energy consumption; optimal insulation thickness; life cycle cost analysis; underground tunnel

Nomenclature

C_0 insulation cost (¥/m)

C_1 electricity cost (¥/m)

C_e electricity price (¥/kWh)

C_t total cost (¥/m)

c_p specific heat capacity of air (kJ/(kgK))

COP coefficient of performance of the cooling system

ΔC_1 difference between the electricity cost with and without insulation (¥/m)

D ratio of down payment to initial investment

d market discount rate

Fo Fourier number ($\alpha_1 t/r_1^2$)

h convection coefficient (W/(m^{2}K))

i energy price rise rate

J_0, J_1 Bessel functions of the first kind of order 0 and 1

k_1 thermal conductivity of rock (W/(mK))

k_2 thermal conductivity of insulation layer (W/(mK))

LCS life cycle saving (¥/m)

M_s ratio of the annual maintenance and operation cost to initial investment

m mass flow rate of air (kg/s)

m' loan interest rate

N payback period (year)

N_L term of loan (year)

N_{min} years over which mortgage payments contribute to the analysis

Ne analysis period (year)

P_1 ratio of cycle cost to the first-year fuel cost

P_2 ratio of life cycle expenditures to the initial investment

PWF present worth factor

Q heat gains of air (kJ)

q heat flux (W/m^2)

q' heat transfer rate per meter (W/m)

R_v ratio of resale value at the end of analysis period to initial investment

r cylindrical coordinate

r_1 radius of tunnel with insulation layer (m)

r_2 radius of tunnel without insulation layer (m)

r_3 radius of outer boundary (m)

T temperature (ºC)

T_a inlet air temperature (ºC)

T_0 original rock temperature (ºC)

T_1 insulation layer temperature (ºC)

T_2 rock temperature (ºC)

t time (s)

ΔT_a air temperature difference between inlet and outlet (ºC)

Y_0, Y_1 Bessel functions of the 2^{ed} kind of order 0 and 1

Greek symbols

α thermal diffusivity (m^2/s)

α_1 thermal diffusivity of rock (m^2/s)

α_2 thermal diffusivity of insulation layer (m^2/s)

β, β_n eigenvalues

δ insulation thickness (m)

subscript

1 insulation layer

2 rock

superscript

(1) unsteady state solution

(2) steady state solution

1. Introduction

The increasing mineral production rate is essential to meet the growing demand of resources due to the rapidly growing population and industrialization [1], which necessitates the extraction of the resources from underground at greater depths. It was reported that the air temperature in the Anglo-gold mine in South Africa was higher than 55 °C with the mining depth exceeding 3800 m. In China, there were more than 74 coal mines with mining depth exceeding 900 m in 2015, and the original rock temperature ranges between 35-45 °C. Recently, an increasing number of coal and metal mines are facing the engineering challenge caused by hot and humid mining environment, which imposes a negative impact on miners' health, mining facilities and productivity [2]. It is imperative for deep mines to provide a suitable working environment through cost effective cooling measures.

Various cooling systems with improved overall efficiency and operation schemes with reduced electricity cost have been adopted to achieve the required thermal environment in underground spaces [3-5]. For instance, the operation scheme of the ice-cooling system was modified according to the peak-valley electricity tariff to reduce the electricity cost [4]. The ground air cooler, chilled water close to 0 °C and ice refrigeration system were used to explore an energy efficient solution for deep mines [6]. Inrushing mine water was used as the source of cooling energy to control the environment, which helped to reduce the energy consumption of the cooling system [7]. The electrical energy consumed by cooling system accounted for more than 20% of total energy consumed by the coal mine. The variable speed drive technology was used to reduce the overall electricity demand, with a total energy consumption reduction of 33% [8, 9]. The thermal-hydraulic characteristics of an integrated mine cooling system was investigated by using a simulation model with a holistic view to assess the system's energy expenditure [10]. It was shown that the comfortable and healthy environment conditions can be created without a significant increase in the capital cost.

Although above investigations indicate that these technologies can reduce the electricity cost, the cooling system's investment and electricity consumption are considerably high for mines. This is because a significant amount of heat transfers from tunnel surrounding rock to the airflow in deep underground space, which leads to a large cooling load. The cooling load can be decreased through thermal insulation of the building envelopes, leading to a reduced investment and electricity cost of the cooling system for residential buildings [11-13]. Intuitively, thermal insulation is applicable to reduce the overall energy consumption of cooling system in underground spaces [14]. Heat transferred from the surrounding rock into underground space may account for more than 75% of total cooling load in deep mines [15]. Therefore, thermal insulation presents the greatest potential in minimizing the cooling requirement and reducing the electricity cost of cooling system [16]. Liu et al. [17] studied the thermal insulation effects through various models based on one-dimensional slab model with Dirichlet or Neumann boundary conditions. Many experimental investigations also indicated that the outlet airflow temperature was obviously decreased when thermal insulation was applied [18-21].

However, greater insulation thickness can increase the materials' costs. An economic assessment should be carried out on the insulation design for a given underground tunnel to identify the economic balance between the decrease in the electricity consumption and the increase in the insulation cost, and such an approach has been broadly adopted in the industrial and residential buildings [22-25]. Ozel et al. [26] investigated the optimum insulation thickness of building walls by using life cycle cost method coupling with the consideration of the environmental impact analysis. Motaghian et al. [27] reported that the optimum insulation arrangements should be determined by employing multi-objective optimization. Dombayci [28] evaluated the environmental impact of the optimal thickness of external wall insulation for buildings and found out that the energy expenditure was reduced by 46.6%. More reduction in heating and cooling loads (86.63%) was achievable when the optimal insulation thickness ranging between 3-5 cm was used to insulate external walls [29]. Kecebas et al. [30] and Erturk et al. [31-33] investigated the optimal insulation thickness of pipes by using life cycle cost method, in which the effect of air gap was considered. The optimal insulation thickness in similar engineering areas was also investigated by Huang et al. [34] using the life cycle cost analysis. Adamczyk et al. [35] proposed that the investment of thermal insulation was beneficial for ecological environment because the energy demand was reduced. Such improvements on the thermal performance economically benefit the application due to the reduced electricity cost. The capital cost associated with the use of thermal insulation can be recovered within a certain period of time. Therefore, the payback period is usually used as a direct measure of the economic benefit of an invested technical improvement [36]. An investment payback period ranged from 1 year to 2.3 years was achieved when the rock wool and polystyrene were used as the insulation material based on the life cycle cost analysis [37]. A shorter payback period was also possible when different configurations were conducted [38, 39].

Researchers have made a tremendous progress in studying the impact of thermal insulation on building. However, the thermal insulation effect, including optimal insulation thickness, life cycle saving and the payback period in deep mines is rarely investigated. Especially, the effect of various rock temperatures on the optimal insulation thickness has not been reported, which indicates that a further investigation on the economic benefit analysis on the thermal insulation effect is needed. This paper is committed to investigating how the cooling load and the total cost are affected by thermal insulation and understanding how to identify the optimal insulation thickness for a given underground tunnel. Firstly, the cylindrical heat conduction model with Robin boundary condition was solved by using the separation-of-variables method. Secondly, based on above analytic results, the effects of insulation thickness, thermal conductivities of insulation layer and rock, tunnel radius and convection coefficient on the heat flux reduction were investigated. Finally, we investigated the optimal insulation thickness, life cycle saving and payback period under various rock temperatures by employing the life cycle cost analysis. The flowchart of this study is shown in Fig. 1.

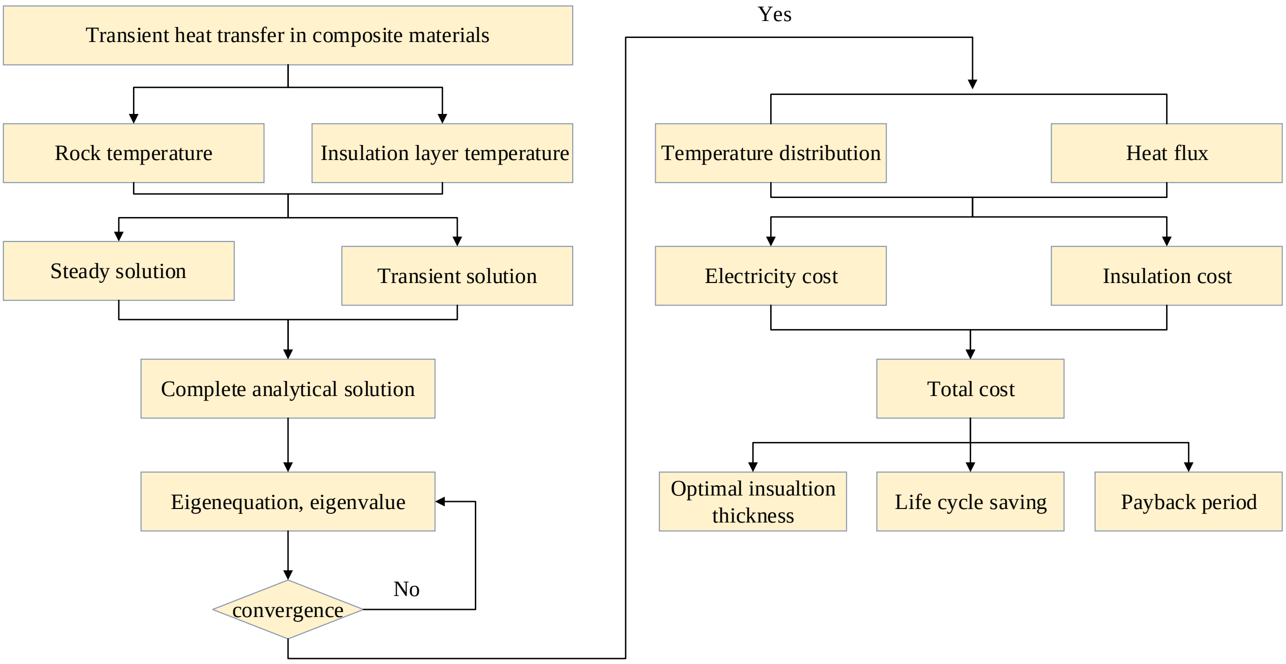

Fig. 1. Flowchart of this study.

2. Mathematical description

2.1. Heat transfer model

2.1.1. Basic equations

When the air flows through the underground tunnel, heat is dissipated from tunnel rock to the airflow driven by the temperature difference. To quantify this heat flux in a practical and reasonable way, the following assumptions are made to facilitate the analytic model [40, 41]: (1) The thermal-physical parameters of tunnel rock and insulation layer are constant, homogeneous and isotropic. (2) The tunnel rock is assumed dry, which means that the mass transfer between rock and airflow is not present. (3) The contact resistance between rock and insulation layer is negligible. (4) The cross-section shape of underground tunnel is circular. Therefore, the schematic diagram of the engineering problem can be illustrated by Fig. 2, which simplifies the heat exchange between the tunnel rock and insulation layer into one-dimensional transient heat conduction process in the cylindrical coordinate.

The governing equation is described by Eq. (1) [42]:

$$\frac{\partial T_i}{\partial t} = \alpha_i \left(\frac{\partial^2 T_i}{\partial r^2} + \frac{1}{r} \frac{\partial T_i}{\partial r} \right) \tag{1}$$

where T is temperature, t is time, r is cylindrical coordinate, α is thermal diffusivity. For the subscript, i=1 represents the insulation layer, and i=2 represents the rock.

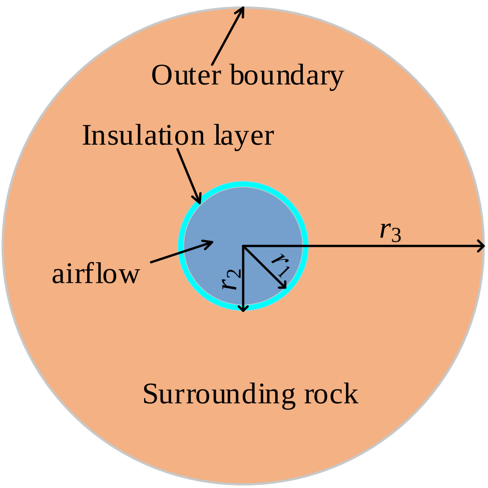

Fig. 2. Schematic of analytic model.

The initial and boundary conditions are given by Eq. (2) and Eq. (3):

$$\begin{cases} T_1(r,0) = T_0 \\ T_2(r,0) = T_0 \end{cases} \tag{2}$$

$$\begin{cases} r = r_3 : T_2\left(r_3, t\right) = T_0 \\ r = r_1 : k_1 \dfrac{\partial T_1}{\partial r} = h\left(T_1 - T_a\right) \end{cases} \tag{3}$$

where T_0 is the initial temperature for both rock and insulation layer; r_1 is the radius of tunnel with insulation layer; r_3 is the radius of outer boundary; T_a is air temperature; k is thermal conductivity.

Because the contact thermal resistance is negligible, the contact boundary condition is described by Eq. (4):

$$r = r_2: \quad \begin{cases} T_1\left(r_2, t\right) = T_2\left(r_2, t\right) \\ k_1 \dfrac{\partial T_1(r_2, t)}{\partial r} = k_2 \dfrac{\partial T_2(r_2, t)}{\partial r} \end{cases} \tag{4}$$

where r_2 is radius of tunnel without insulation layer.

2.1.2. Analytic solution

The Eqs. (1)-(4) are solved by using the variable-separation-method [43]. The detailed process is shown in the Appendix. The analytic solution is described by Eq. (5) and Eq. (6):

$$T_1^{(1)}(r,t) = \sum_{n=1}^{\infty} A_{1n}\left[J_0\left(\frac{\beta_n}{\sqrt{\alpha_1}} r\right) + \frac{B_{1n}}{A_{1n}} Y_0\left(\frac{\beta_n}{\sqrt{\alpha_1}} r\right)\right] \cdot \exp(-\beta_n^2 t) \tag{5}$$

$$T_2^{(1)}(r,t) = \sum_{n=1}^{\infty} A_{1n}\left[\frac{A_{2n}}{A_{1n}} J_0\left(\frac{\beta_n}{\sqrt{\alpha_2}} r\right) + \frac{B_{2n}}{A_{1n}} Y_0\left(\frac{\beta_n}{\sqrt{\alpha_2}} r\right)\right] \cdot \exp(-\beta_n^2 t) \tag{6}$$

The derivation of Eq. (5) and Eq. (6) can be obtained according to derivatives of *Bessel* function:

$$\frac{\partial T_1^{(1)}(r,t)}{\partial r} = -\sum_{n=1}^{\infty} A_{1n} \cdot \exp(-\beta_n^2 t) \frac{\beta_n}{\sqrt{\alpha_1}}\left[J_1\left(\frac{\beta_n}{\sqrt{\alpha_1}} r\right) + B_{1n}^{'} Y_1\left(\frac{\beta_n}{\sqrt{\alpha_1}} r\right)\right] \tag{7}$$

$$\frac{\partial T_2^{(1)}(r,t)}{\partial r} = -\sum_{n=1}^{\infty} A_{1n} \cdot \exp(-\beta_n^2 t) \frac{\beta_n}{\sqrt{\alpha_2}}\left[A_{2n}^{'} J_1\left(\frac{\beta_n}{\sqrt{\alpha_2}} r\right) + B_{2n}^{'} Y_1\left(\frac{\beta_n}{\sqrt{\alpha_1}} r\right)\right] \tag{8}$$

where, $B_{1n}^{'} = B_{1n} / A_{1n}$, $B_{2n}^{'} = B_{2n} / A_{1n}$, $A_{2n}^{'} = A_{2n} / A_{1n}$.

The boundary condition at $r=r_1$ is transformed to Eq. (9):

$$-k_1 \frac{\beta_n}{\sqrt{\alpha_1}} J_1\left(\frac{\beta_n}{\sqrt{\alpha_1}} r\right) - hJ_0\left(\frac{\beta_n}{\sqrt{\alpha_1}} r_1\right) = B'_{1n}\left[hY_0\left(\frac{\beta_n}{\sqrt{\alpha_1}} r_1\right) + k_1 \frac{\beta_n}{\sqrt{\alpha_1}} Y_1\left(\frac{\beta_n}{\sqrt{\alpha_1}} r\right) \right] \tag{9}$$

In addition, the boundary conditions at $r=r_2$ and $r=r_3$ are changed to:

$$\begin{cases} A'_{2n} J_0\left(\frac{\beta_n}{\sqrt{\alpha_2}} r_3\right) + B'_{2n} Y_0\left(\frac{\beta_n}{\sqrt{\alpha_2}} r_3\right) = 0 \\ A'_{2n} J_0\left(\frac{\beta_n}{\sqrt{\alpha_2}} r_2\right) + B'_{2n} Y_0\left(\frac{\beta_n}{\sqrt{\alpha_2}} r_2\right) = J_0\left(\frac{\beta_n}{\sqrt{\alpha_1}} r_2\right) + B'_{1n} Y_0\left(\frac{\beta_n}{\sqrt{\alpha_1}} r_2\right) \end{cases} \tag{10}$$

Then, the coefficients of A'_{2n}, B'_{2n} are computed and described by Eq. (11):

$$\begin{bmatrix} A'_{2n} \\ B'_{2n} \end{bmatrix} = \begin{bmatrix} J_0\left(\frac{\beta_n}{\sqrt{\alpha_2}} r_3\right) & Y_0\left(\frac{\beta_n}{\sqrt{\alpha_2}} r_3\right) \\ J_0\left(\frac{\beta_n}{\sqrt{\alpha_2}} r_2\right) & Y_0\left(\frac{\beta_n}{\sqrt{\alpha_2}} r_2\right) \end{bmatrix}^{-1} \begin{bmatrix} 0 \\ J_0\left(\frac{\beta_n}{\sqrt{\alpha_1}} r_2\right) + B'_{1n} Y_0\left(\frac{\beta_n}{\sqrt{\alpha_1}} r_2\right) \end{bmatrix} \tag{11}$$

Consequently, the eigenequation is obtained as:

$$\frac{k_1}{\sqrt{\alpha_1}} \cdot \begin{bmatrix} 1 & B'_{1n} \end{bmatrix} \cdot \begin{bmatrix} J_1\left(\frac{\beta_n}{\sqrt{\alpha_1}} r_2\right) \\ Y_1\left(\frac{\beta_n}{\sqrt{\alpha_1}} r_2\right) \end{bmatrix} - \frac{k_2}{\sqrt{\alpha_2}} \cdot \begin{bmatrix} A'_{2n} & B'_{2n} \end{bmatrix} \cdot \begin{bmatrix} J_1\left(\frac{\beta_n}{\sqrt{\alpha_2}} r_2\right) \\ Y_1\left(\frac{\beta_n}{\sqrt{\alpha_2}} r_2\right) \end{bmatrix} = 0 \tag{12}$$

The eigenequation is a transcendental equation, which can only be solved through numerical measure. The eigenvalues are calculated by employing MATLAB in this study, and the solution's convergence is also investigated. The analytic solution does not converge when the first 15 eigenvalues are used. The analytic solution converges when the first 30 eigenvalues are employed, which is consistent with the solution of using the first 500 eigenvalues. Therefore, the first 30 eigenvalues are used for the following computation.

The coefficients of $B'_{1n}, A'_{2n}, B'_{2n}$ are calculated by using the eigenvalues, and A_{1n} is determined by the initial condition presented in Eq. (A10). Substituting the general solution into the initial condition, Eq. (13) is obtained as:

$$\begin{cases} T_1^{(1)}(r,0)=\sum_{n=1}^{\infty}A_{1n}\left[J_0(\frac{\beta_n}{\sqrt{\alpha_1}}r)+B_{1n}^{'}Y_0(\frac{\beta_n}{\sqrt{\alpha_1}}r)\right]=\sum_{n=1}^{\infty}A_{1n}\varphi_{1n}(r) \\ T_2^{(1)}(r,0)=\sum_{n=1}^{\infty}A_{1n}\left[A_{2n}^{'}J_0(\frac{\beta_n}{\sqrt{\alpha_2}}r)+B_{2n}^{'}Y_0(\frac{\beta_n}{\sqrt{\alpha_2}}r)\right]=\sum_{n=1}^{\infty}A_{1n}\varphi_{2n}(r) \end{cases} \quad (13)$$

where, $\varphi_{1n}(r)=J_0(\frac{\beta_n}{\sqrt{\alpha_1}}r)+B_{1n}^{'}Y_0(\frac{\beta_n}{\sqrt{\alpha_1}}r)$, $\varphi_{2n}(r)=A_{2n}^{'}J_0(\frac{\beta_n}{\sqrt{\alpha_2}}r)+B_{2n}^{'}Y_0(\frac{\beta_n}{\sqrt{\alpha_2}}r)$.

The orthogonal expression for $\varphi_{1n}(r)$ and $\varphi_{2n}(r)$ is described by Eq. (14):

$$\sum_{i=1}^{2}\frac{k_i}{\alpha_i}\int_{r_i}^{r_{i+1}} r\varphi_{1n}(r)\varphi_{2n}(r)dr=\begin{cases} 0 & m\neq n \\ N_n & m=n \end{cases} \quad (14)$$

where, $N_n=\sum_{i=1}^{2}\frac{k_i}{\alpha_i}\int_{r_i}^{r_{i+1}} r\varphi_{in}^2(r)dr$.

From Eq. (14), Eq. (15) can be obtained:

$$\frac{k_1}{\alpha_1}\int_{r_1}^{r_2}T_1^{(1)}(r,0)\cdot r\cdot\varphi_{1n}(r)dr+\frac{k_2}{\alpha_2}\int_{r_2}^{r_3}T_2^{(1)}(r,0)\cdot r\cdot\varphi_{2n}(r)dr=A_{1n}\left[\frac{k_1}{\alpha_1}\int_{r_1}^{r_2}r\cdot\varphi_{1n}^2(r)dr+\frac{k_2}{\alpha_2}\int_{r_2}^{r_3}r\cdot\varphi_{2n}^2(r)dr\right] \quad (15)$$

The coefficient A_{1n} is shown as:

$$A_{1n}=\frac{1}{N_n}\left[\frac{k_1}{\alpha_1}\int_{r_1}^{r_2}T_1^{(1)}(r,0)\cdot r\cdot\varphi_{1n}(r)dr+\frac{k_2}{\alpha_2}\int_{r_2}^{r_3}T_2^{(1)}(r,0)\cdot r\cdot\varphi_{2n}(r)dr\right] \quad (16)$$

2.2. Life cycle cost method

The economic benefit of thermal insulation is investigated by adopting the life cycle cost (LCC) analysis, which is a widely used method for evaluating all relevant costs over the life cycle time [22, 30, 39, 44]. The main procedures of LCC analysis are described as follows: (1) The initial cost is calculated. (2) The operation cost is evaluated when the influences of inflation and interest rate are considered. (3) The minimum total cost is then determined to provide the optimal insulation thickness. (4) The payback period and the life cycle saving are obtained.

2.2.1. *Insulation cost*

The lightweight geopolymer concrete (LGC) with lower greenhouse gas emission is used as the insulation material in this study. The LGC with thermal conductivity of 0.1 W/(mK) and dry density of 450 kg/m^3 was produced by using fly ash and alkali solution at room temperature [45]. The price of insulation layer is about 325 ¥/m^3 (¥: RMB). The insulation cost per tunnel length under various insulation thicknesses is calculated.

Fig. 3 indicates that the insulation cost is approximately linearly increased when the insulation thickness increases from 0 m to 0.3 m. For instance, the insulation cost increases from 81.25 ¥/m to 1317 ¥/m when the insulation thickness increases from 0.02 m to 0.3 m. The empirical correlation between the insulation cost and the insulation thickness can be described by Eq. (17):

$$C_0 = -11.31 + 4382.93 \times \delta \tag{17}$$

where C_0 is the insulation cost per tunnel length. δ is the insulation thickness.

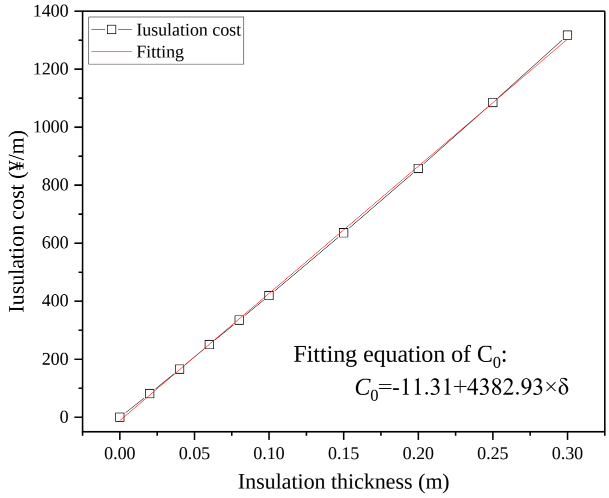

Fig. 3. The insulation cost versus thickness of insulation layer

2.2.2. *Annual electricity cost*

The annual electricity cost (C_1) is dependent on the total heat gain of the airflow. Due to the unsteady process of the convective heat transfer, the annual heat gain (cooling load) is calculated by the integration method:

$$Q = m \cdot \int_{0}^{365\times24\times3600} c_p \cdot \Delta T_{\mathrm{a}} dt \tag{18}$$

where Q is the heat gain of air, c_p is the specific heat capacity of air, m is the mass flow rate, ΔT_{a} is the temperature difference between inlet and outlet air.

The economic evaluation can be carried out through the P_1-P_2 economical method, which is shown as follows [34]:

$$P_1 = PWF(Ne,i,d) = \sum_{j=1}^{N_e} \frac{(1+i)^{j-1}}{(1+d)^j} = \begin{cases} \frac{1}{d-i}[1-(\frac{1+i}{1+d})^{Ne}], i \neq d \\ \frac{Ne}{1+i}, i = d \end{cases} \tag{19}$$

$$P_2 = D + (1-D)\frac{PWF(N_{\mathrm{min}},0,d)}{PWF(N_{\mathrm{L}},0,m')} + M_s \times PWF(Ne,i,d) - \frac{R_v}{(1+d)^{Ne}} \tag{20}$$

where P_1 is the ratio of life cycle cost to the first-year electricity cost. P_2 is the ratio of life cycle expenditures to the initial investment. PWF is the present worth factor. Ne is the analysis period, year. N_{L} is the term of loan, year. d is the market discount rate. i is the energy price rise rate. m' is the loan interest rate. N_{min} is the number of years over which mortgage payments contribute to the analysis (usually the minimum of Ne and N_{L}). M_{s} is the ratio of the annual maintenance and operation cost to initial investment. R_{v} is the ratio of resale value at the end of analysis period to initial investment. D is the ratio of down payment to initial investment.

The annual electricity cost C_1 is calculated by Eq. (21):

$$C_1 = \frac{Q}{3600 \times 250 \times \mathrm{COP}} C_{\mathrm{e}} \tag{21}$$

where COP is the coefficient of performance, C_{e} is the electricity price. All the parameters and their values are listed in Table 1.

Table 1 Parameter for the life cycle cost analysis.

Parameters	Values
Interest rate (*i*)	8%
Lifetime (*Ne*)	10 Years
Market discount rate (*d*)	6%
Coefficient of Performance (COP)	2.8
Electricity price (C_e)	1 ¥/kWh

The heat gain of airflow from the tunnel with a length of 250 m, wind speed of 1 m/s, original surrounding rock temperature ranging from 35 ºC to 45 ºC, inlet air temperature of 20 ºC and tunnel radius of 2 m is calculated after the tunnel is ventilated for 12 months. The heat gain of airflow and the annual electricity cost of the cooling system with different insulation thicknesses are listed in Table 2. It is observed that the heat gain of airflow and the annual electricity cost per meter decrease from 1844 MJ/m to 897 MJ/m and from 183 ¥/m to 89 ¥/m respectively when the insulation thickness increases from 0 to 0.3 m.

Table 2 Annual electricity cost versus insulation thickness.

Insulation thickness (m)	0	0.04	0.08	0.1	0.15	0.2	0.25	0.3
Heat gains (MJ/m)	1844	1640	1467	1394	1216	1086	983	897
Annual electricity cost (¥/m)	183.0	162.7	145.6	138.3	120.6	107.7	97.5	89.0

Fig. 4 shows the influence of rock temperature on the annual electricity cost under various insulation thickness. The annual electricity cost is observed to be decreased with the increased insulation thickness. It is known that the heat transfer can be significantly reduced by a larger insulation thickness, thereby giving a reduced cooling load, which then leads to a lower annual electricity cost. The empirical correlations between the annual electricity cost and the insulation thickness under various rock temperatures ranging from 35 °C to 45 °C are also presented in Fig. 4.

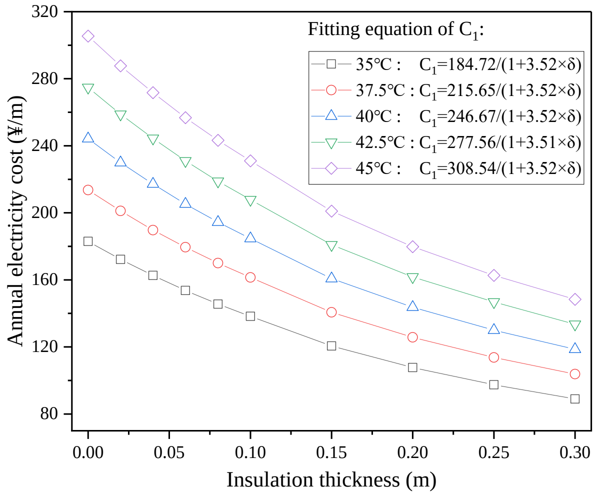

Fig. 4. Annual electricity cost under various original rock temperature.

2.2.3. Total cost, life cycle saving and payback period

The total cost (C_t) consists of the electricity cost over the life time and the insulation cost, which can be described by Eq. (22):

$$C_t = P_1 C_1 + P_2 C_0 \tag{22}$$

Life cycle saving (LCS) is the difference between the saved energy cost over the life cycle time and the insulation cost, which can be calculated by Eq. (23):

$$\text{LCS} = P_1 \Delta C_1 - P_2 C_0 \tag{23}$$

where ΔC_1 is the electricity cost difference with and without the insulation layer.

By setting Eq. (23) to zero, the payback period N can be calculated:

$$N = \begin{cases} \dfrac{\text{In}[1\text{-}((P_2 \times C_0)/(\Delta C_1)) \times (d\text{-}i)]}{\text{In}((1+i)/(1+d))}, i \neq d \\ ((P_2 \times C)/(\Delta C_1)) \times (1+i), i = d \end{cases} \tag{24}$$

3. Results and discussion

3.1. Verification of analytic solution

A numerical model is simulated by ANSYS Fluent 18.0 to verify the analytic solution. The quadrilateral mesh with high quality is created through ICEM CFD (Integrated Computer Engineering and Manufacturing code for Computational Fluid Dynamics). To decrease the total mesh number and shorten the computing time, uniform grid is employed in the insulation layer and nonuniform grid is used in surrounding rock region, respectively.

The key thermal properties and boundary conditions are listed in Table 3. The thermal properties of tunnel and ventilation parameters are obtained from a coal mine in Xuzhou, China. The properties of an insulation material are provided by a literature [45]. The thermal penetration length is defined as the depth at which the dimensionless temperature $(T - T_a)/(T_0 - T_a)$ inside the surrounding rock reduces to 0.99 based on the boundary layer theory [46]. To eliminate the boundary effect, the outer boundary radius should be larger than the thermal penetration length [18, 40]. The analytic analysis indicated that the outer boundary radius in Table 3 is larger than the thermal penetration depth, which is not discussed in this paper. The grid independence investigation is conducted on this numerical model. Four grids with mesh numbers of 7900, 14220, 20856 and 33812 are generated, respectively. The rock temperature distribution under different meshing are compared when the tunnel is ventilated for about ten days (Fo=0.28), as shown in Fig. 5 (a). It is seen that the calculated rock temperature does not vary when the grid number increased to 20856. To minimise the computational time without compromising the calculation accuracy, the mesh with the grid number of 20856 is employed for the following investigation.

Table 3 Key thermal properties and boundary conditions.

Parameters	Value
Original rock temperature, T_0	35 °C
Thermal conductivity of rock (TCR), k_1	2.4 W/(mK)
Thermal diffusivity of rock, α_1	1.3×10^{-6} m²/s
Tunnel radius, r_1	2 m
Convection coefficient, h	20 W/(m²K)
Inlet air temperature, T_a	20 °C
Thermal conductivity of insulation layer (TCIL), k_2	0.1 W/(mK)
Thermal diffusivity of insulation layer, α_2	0.4×10^{-6} m²/s
Outer boundary radius, r_3	30 m
Insulation thickness, δ ($\delta=r_2-r_1$)	0.1 m

The temperature distribution calculated from the analytic solution when Fo=0.28, Fo=5.05 and Fo=10.11 are compared with that given by Fluent, as shown in Fig. 5 (b). The tunnel surface temperature difference between analytic and Fluent is 0.18 °C, 0.23 °C and 0.03 °C when Fo=0.28, 5.05 and 10.11 respectively, which shows that the analytic results are in good agreement with the numerical results. Starfield et al. [47] and Liu et al. [17] computed rock temperature when the tunnel rock is dry. The rock temperature is also solved through the analytic solution in this study and the comparison of rock temperature distribution is presented in Fig. 5 (c). The tunnel surface temperature of Starfield's, Liu's, analytic and ANSYS solution is 30.73 °C, 30.89 °C, 30.75 °C and 30.75 °C respectively when Fo=18.9. The maximum relative error is lower than 0.46%. Therefore, the validity of the analytic solution in this study can be proved.

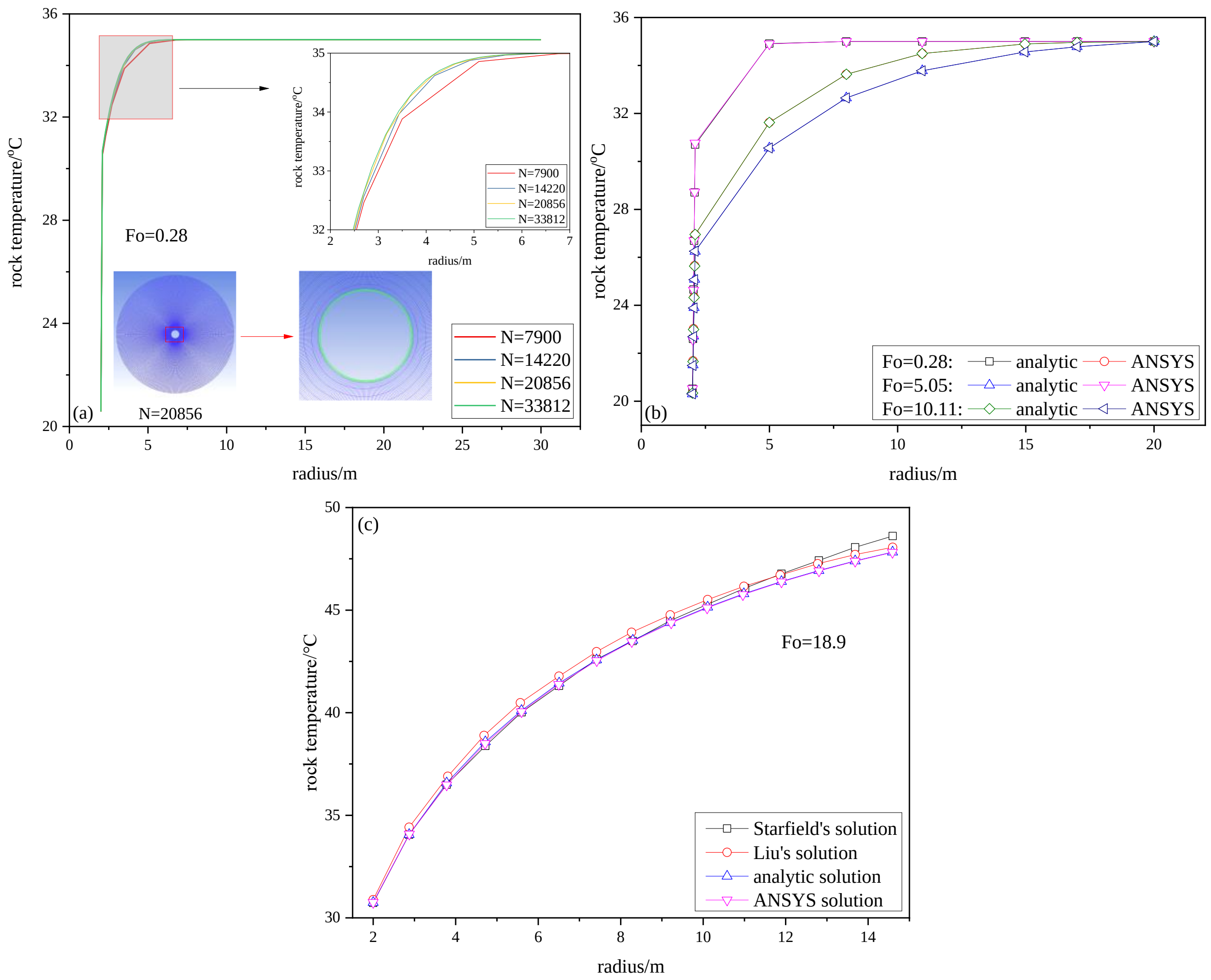

Fig. 5. Model validation: (a) grid independence verification, analytic solution versus (b) ANSYS and (c) literatures' results.

3.2. Thermal insulation effect

3.2.1. Rock temperature

The rock temperature distributions in the cross section of the tunnel without and with insulation layer are investigated, as shown in Fig. 6. As can be seen from Fig. 6 (a), the rock temperature considerably decreases near the tunnel wall due to the cooling effect caused by the airflow with lower temperature. Such cooling effect weakens as it moves further away from the tunnel wall. The rock temperature stays almost at a constant level when the distance is above a certain threshold, which is the length of the outer boundary that needs to be determined in the analytic model. The rock temperature is expected to decrease rapidly at the initial stage due to the transient heat transfer process. After a period of time, the reducing rate of the rock temperature decreases gradually. For instance, the tunnel surface temperature decreases from 35 ºC to 20.90 ºC when Fo increases from 0 to 0.84, with a temperature difference of 14.10 ºC. In contrast, the rock temperature difference only reduces by 0.83 ºC when Fo increases from 0.84 to 10.11. This is because that the temperature difference between airflow and tunnel is reduced by the increased Fo number. Similar rock temperature distribution is achieved by Wang et al. [40, 48] through experimental and analytic investigations.

Fig. 6 (b) presents the rock temperature distribution of tunnel with insulation layer. It is seen that the temperature gradient in insulation layer is significantly larger than that in surrounding rock. This is because that the TCIL is smaller than that of surrounding rock. For instance, the temperature gradient in insulation layer is 101.79 ºC/m, in comparison with that of 8.47 ºC/m in surrounding rock at Fo=0.28. The temperature gradient in the insulation layer also decreases when the Fo number increases, which is caused by the reduced temperature difference between airflow and tunnel. As we can also see from Fig. 6, the temperature gradient near the tunnel wall is large, which suggests that the closer the distance to the tunnel wall, the higher the heat flux is [49, 50]. Therefore, an excellent thermal insulation performance can be achieved when the insulation layer is installed on the tunnel wall [42].

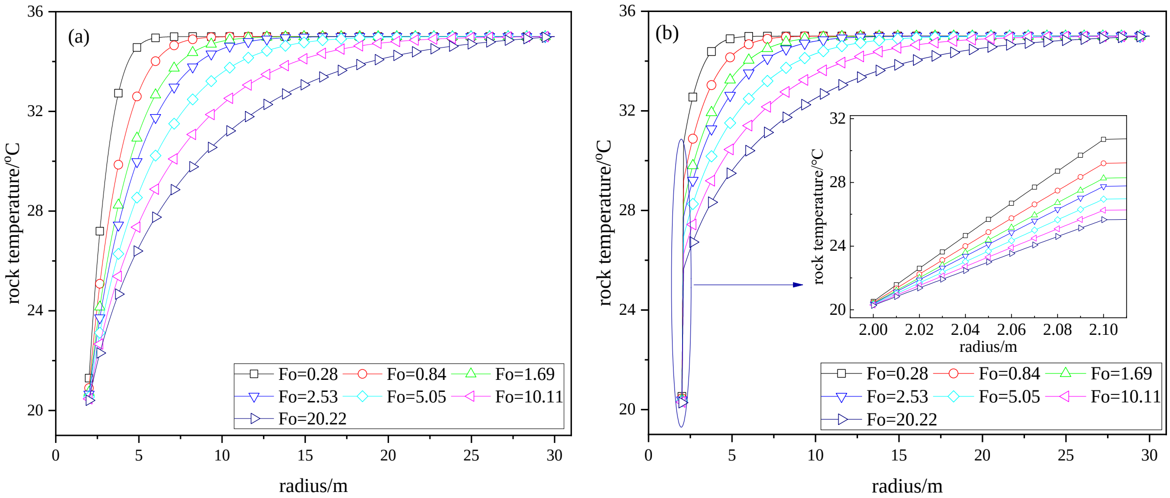

Fig. 6. Rock temperature of tunnel (a) without and (b) with insulation layer.

To verify the thermal insulation effect, the surplus temperature is monitored during the unsteady heat transfer process. The surplus temperature is defined by the temperature difference between tunnel wall and airflow, which can be used to compute the heat convection between tunnel and airflow [42]. The variation of surplus temperature with Fo is listed in Table 4, which shows that the surplus temperature of original tunnel is always higher than that of insulated tunnel. Although the surplus temperature's ratio decreases gradually when the Fo increases, the heat convection of original tunnel is still about 1.43 times higher than that of insulated tunnel when Fo=20.22. It indicates that thermal insulation can reduce about 30% of total heat convection when the tunnel is ventilated for two years. Therefore, the thermal insulation can considerably reduce heat convection between tunnel and airflow, which contributes to the decreased cooling load.

Table 4 Surplus temperature versus Fo number.

Fo	0.28	0.84	1.69	2.53	5.05	10.11	20.22
Original tunnel (°C)	1.30	0.90	0.73	0.65	0.55	0.47	0.40
Insulated tunnel (°C)	0.52	0.45	0.40	0.38	0.34	0.30	0.28

ratio	2.50	2.00	1.83	1.71	1.62	1.57	1.43

3.2.2. Heat flux reduction

Because the thermal insulation effect is dependent on the parameters related to insulation layer, tunnel and ventilation conditions, it is necessary to investigate the impact of insulation thickness, TCIL, TCR, tunnel radius and convection coefficient on thermal insulation effect. A series of calculations of heat flux of the tunnel with/without insulation layer have been conducted under various parameters. Therefore, the effects of these various parameters on heat flux reduction are presented. Because the moisture leads to an increased TCIL and a coupled heat and mass transfer, the thermal insulation effect can be considerably reduced by moisture transfer [45]. Therefore, it may not be feasible for wet tunnel to control underground environment by using thermal insulation, which is not discussed in this study.

Fig. 7 shows the changes of heat flux reduction achieved by various parameters, such as insulation thickness, TCIL, TCR, tunnel radius and convection coefficients. The impact of insulation thickness on heat flux reduction is shown in Fig. 7 (a). Taking the profile under Fo=0.84 as an example, it is found that the heat flux reduction increases when a thicker insulation is used, which indicates that larger insulation thickness can weaken the heat transfer from tunnel rock to airflow. For instance, the heat flux reduction increases from 27.0% to 50.1% when the insulation thickness increases from 0.04 m to 0.1 m. However, larger insulation thickness implicates an increased insulation cost. A balance needs to be achieved among them to achieve the best cost effectiveness, which is discussed in more details in section 3.3. Fig. 7 (b) shows that the heat flux reduction increases when the TCIL decreases. Zhou et al. [51] also found that the heat flux reduction non-linearly decreased with the increased TCIL, which is similar with the variation presented in Fig. 7 (b).This is because a lower TCIL can result in a larger thermal resistance [42]. As the heat flux reduction is strongly dependent on the TCIL, preference should be given to the insulation layer with a lower thermal conductivity. Zhang et al. [52] also indicates that a smaller TCIL can lead to a lower heat flux and a better thermal insulation effect.

Fig. 7 (c) illustrates the impact of TCR on the heat flux reduction with insulation thickness of 0.1 m and TCIR of 0.1 W/(mK). It is seen that an increase in the TCR contributes to an enhancement in heat flux reduction, suggesting that the thermal insulation effect is significant when the TCR is high. For instance, the heat flux reduction increases from 43.6% to 68.0% when the TCR is increased from 1.9 W/(mK) to 4.9 W/(mK). Zhu [19] indicated that an increase in TCR (thermal diffusivity) could lead to a quicker decrease in rock temperature, which is consistent with a larger heat flux reduction. It is known that a higher TCR is equivalent to a smaller thermal resistance of surrounding rock. When the thermal resistance of the surrounding rock is coupled with that of the insulation layer, the smaller the thermal resistance of the surrounding rock, the larger the increasing rate of total thermal resistance is. Therefore, one can expect that a higher TCR coupled with the insulation layer can lead to a significant thermal insulation effect. The influence of the tunnel radius on the heat flux reduction with an insulation thickness of 0.1 m and TCIR of 0.1 W/(mK) is shown in Fig. 7 (d), from which we can find that the heat flux reduction decreases when the tunnel radius increases. This indicates that the thermal insulation effect is significant when the tunnel radius is smaller. The reason is that the total thermal resistance is increased by the decreased tunnel radius. Compared with the tunnel with a small radius, a thicker insulation layer (or smaller TCIL) can achieve the same thermal insulation effect for those tunnels with a large radius.

Fig. 7 (e) shows the impact of convection coefficient on the heat flux reduction. It can be observed that the heat flux reduction is not strongly dependent on the convection coefficient. For instance, the heat flux reduction only increases from 46.3% to 50.3% when the convection coefficient increases from 10 W/(m^2K) to 40 W/(m^2K). The heat transfer can be enhanced by increased convection coefficient. However, the decreased tunnel surface temperature also leads to a reduced temperature difference between tunnel and airflow. This indicates that the increase in the convection coefficient is offset by the decrease in the temperature difference. Therefore, the thermal insulation effect does not significantly depend on the convection coefficient. Zhang [18] experimentally proved that the dimensionless rock temperature was not strongly dependent on the Bi number (convection coefficient), which is consistent with the results showed in Fig. 7 (e). As we can see from the profiles shown in Fig. 7, all these effects of insulation thickness, TCIL, TCR, tunnel radius and convection coefficient on the heat flux reduction are non-linear.

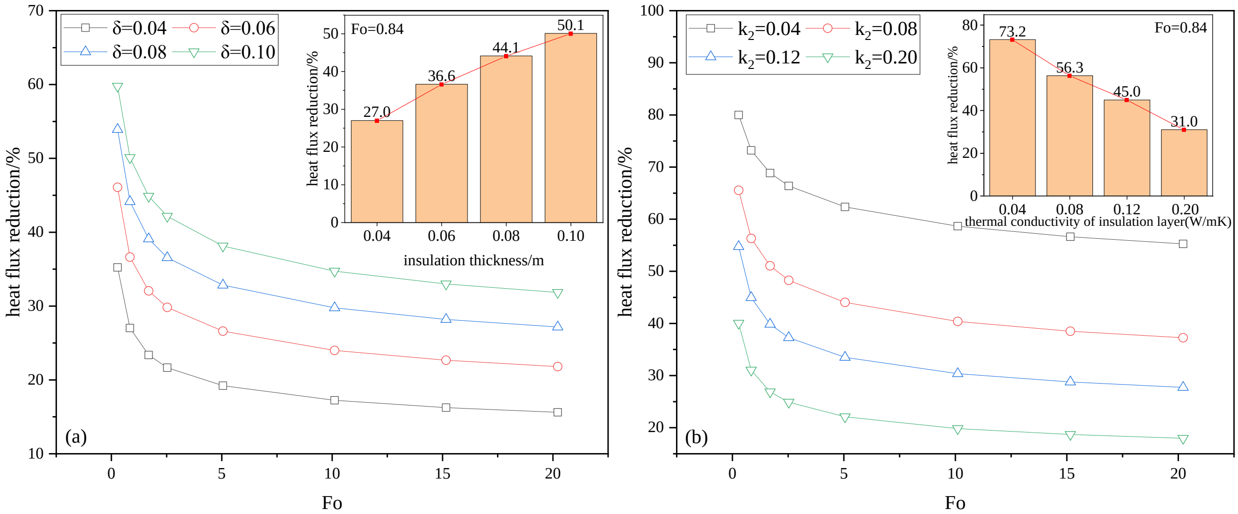

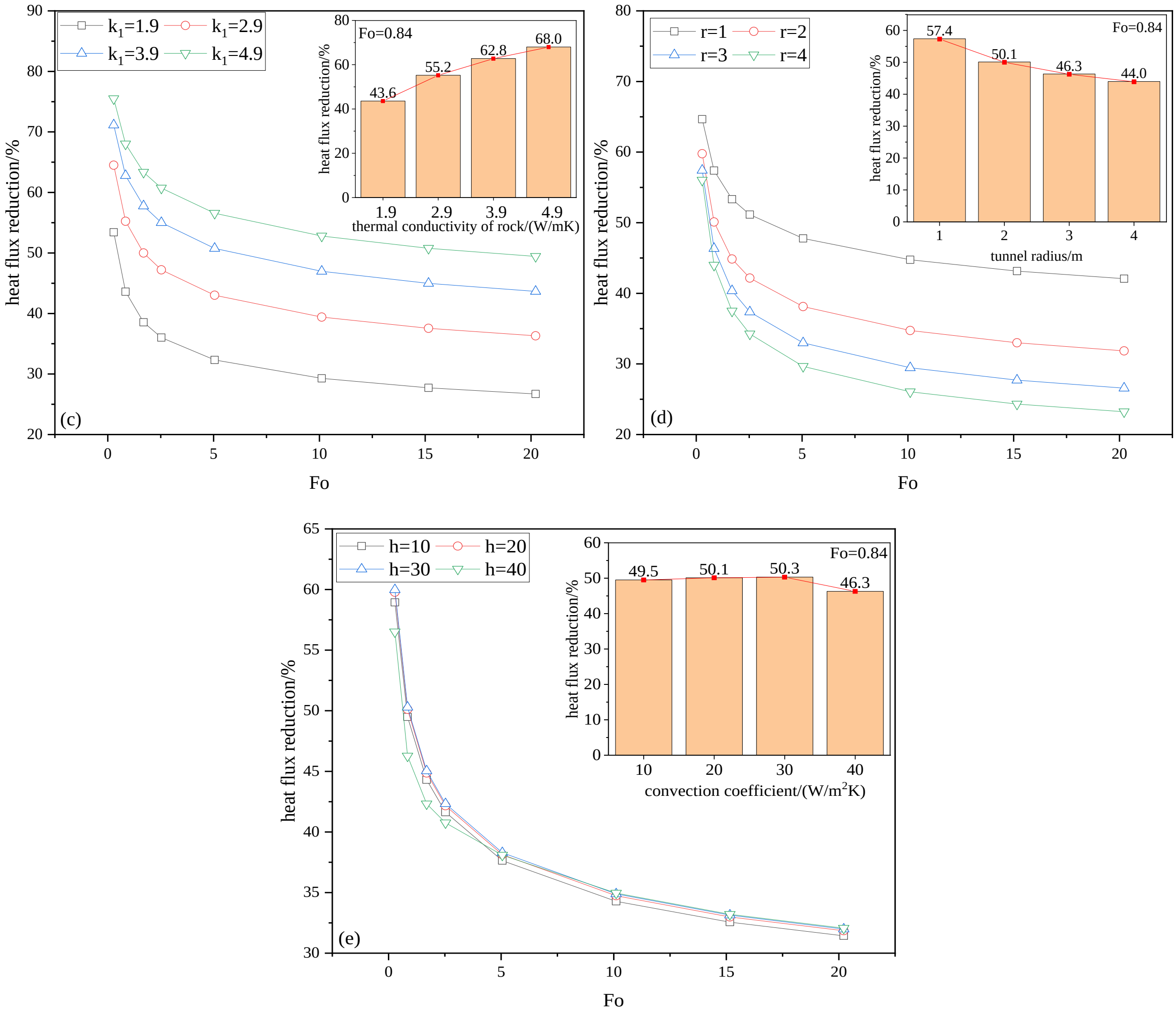

Fig. 7. Heat flux reduction versus (a) insulation thickness, (b) TCIL, (c) TCR, (d) tunnel radius, (e) convection coefficient.

3.3.Economic benefit analysis

3.3.1. Total cost

The insulation cost, electricity cost and the total cost under different insulation thicknesses are calculated based on the life cycle cost method. The effect of insulation thickness on the total cost is presented in Fig. 8. It is seen from Fig. 8 that the total cost firstly decreases and then increases when the insulation thickness increases. For instance, the total cost decreases from 1887 ¥/m to 1820 ¥/m when the insulation thickness increases from 0 m to 0.07 m. The total cost begins to increase when the insulation thickness is larger than 0.07 m. It is known that the optimum insulation thickness should be determined against the lowest total cost [53]. Therefore, the optimal insulation thickness is 0.07 m when the rock temperature is 35 ºC, with the lowest total cost of 1820 ¥/m.

It is also found from Fig. 8 that the electricity cost decreases slowly with the increased insulation thickness. The reason for this phenomenon may attributed to the fact that the thermal conductivity of insulation layer is not small enough to reduce more heat dissipation from tunnel to the airflow. One can expect that the insulation layer with lower thermal conductivity can lead to a remarkable reduction in the electricity cost. In addition, the thermal insulation effect for the tunnel with higher rock temperature may be more significant, which can be proved through the results shown in Fig. 4.

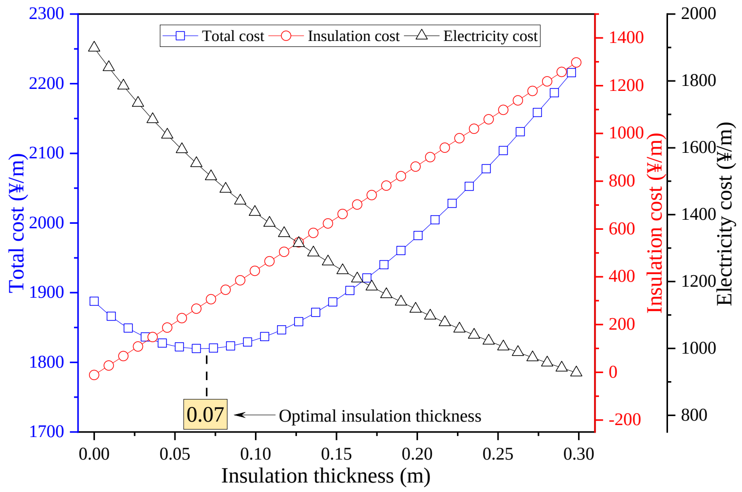

Fig. 8. Total cost versus the insulation thickness (rock temperature=35 ºC).

In order to investigate the influence of rock temperature on the optimal insulation thickness, the total costs under various rock temperatures are also evaluated and shown in Fig. 9. It is found that an increase in the rock temperature can lead to an increase in the total cost. Under the same insulation thickness, the larger the rock temperature, the higher the total cost is. In addition, the optimal insulation thickness is observed to be increased when the rock temperature increases. For instance, the optimal insulation thickness increases from 0.07 m to 0.17m when the rock temperature increases from 35 ºC to 45 ºC. This may be attributed to the fact that a larger insulation thickness is needed to reduce the cooling load for the case with a higher rock temperature.

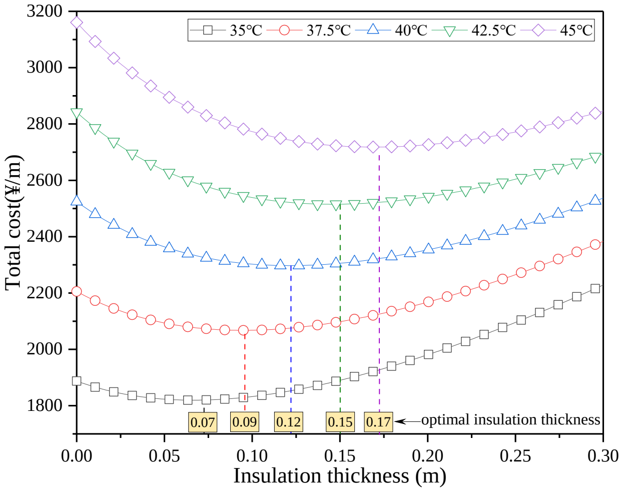

Fig. 9. Total cost versus the insulation thickness (various rock temperatures)

3.3.2. life cycle saving and payback period

The effect of the rock temperature on the life cycle saving is investigated and presented in Fig. 10. It is seen from Fig. 10 (a) that the life cycle saving firstly increases and then decreases when the insulation thickness increases, which indicates that there is a maximum life cycle saving for various cases with different rock temperatures. As shown in Fig. 10 (b), the maximum life cycle savings per tunnel length are 61.2 ¥/m, 128.2 ¥/m, 213.2 ¥/m, 310.1 ¥/m and 421.8 ¥/m when the rock temperature is 35 ºC, 37.5 ºC, 40 ºC, 42.5 ºC and 45 ºC, respectively. In addition, it is also observed from Fig. 10 that the optimal insulation thicknesses corresponding to the maximum life cycle saving under various rock temperatures are consistent with the optimal insulation thickness illustrated in Fig. 9.

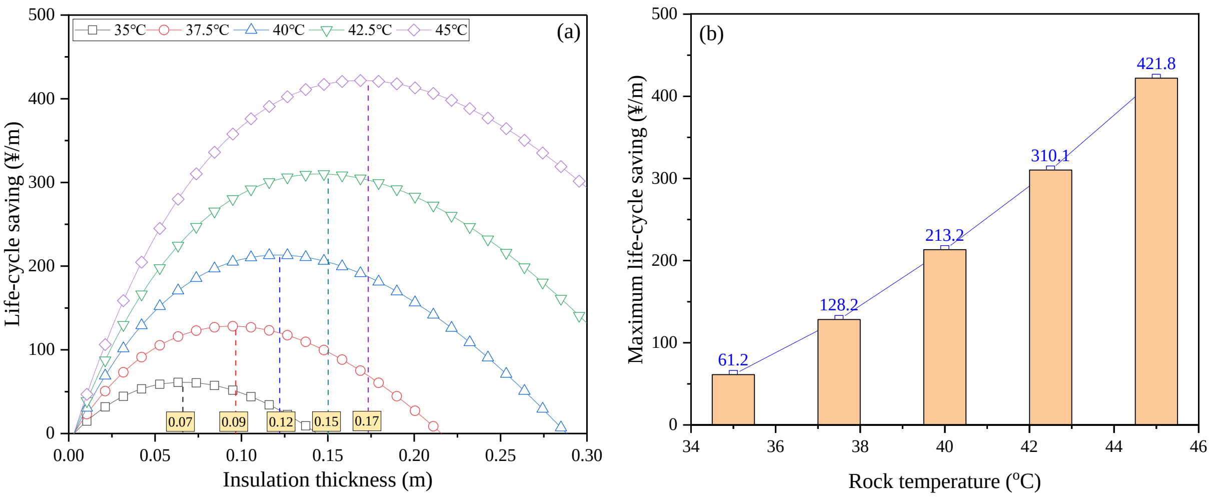

Fig. 10. Life cycle saving versus (a) insulation thickness, (b) rock temperature.

The optimal insulation thickness, maximum life cycle saving and payback period are listed in Table 5. It is found that the optimal insulation thickness and maximum life cycle saving increase from 0.07 m and 61.2 ¥/m to 0.17 m and 421.8 ¥/m when the rock temperature increases from 35 °C to 45 °C. Interestingly, a shorter payback period is achieved by the increased rock temperature. For instance, the payback period reduces from 9.96 years to 4.91 years when the rock temperature increases from 35 °C to 45 °C.

Table 5 Optimal insulation thickness, maximum life cycle saving and payback period under various rock temperatures.

Rock temperature (°C)	**Optimal insulation thickness (m)**	**Maximum life cycle saving (¥/m)**	**Payback period (year)**
35°C	0.07	61.2	9.96
37.5°C	0.09	128.2	8.3
40°C	0.12	213.2	6.85

42.5°C	0.15	310.1	5.72
45°C	0.17	421.8	4.91

4. Conclusions

The transient heat conduction model of insulated underground tunnel is solved by using the separation-of-variable method in this study. The rock temperature and heat flux reduction achieved by applying thermal insulation are investigated. In addition, the optimal thickness, life cycle saving and payback period are discussed based on the life cycle cost method. The main findings are as follows:

(1) The temperature gradient in the insulation layer is considerably larger than that in surrounding rock. The surplus temperature of original tunnel is 2.5-1.43 times higher than that of tunnel with insulation layer when Fo increases from 0.28 to 20.22.

(2) An increase in the insulation thickness and TCR results in an increase in the heat flux reduction. A decrease in TCIL and tunnel radius have a positive impact on the heat flux reduction. The heat flux reduction is not strongly dependent on the convection coefficient.

(3) The total cost firstly decreases and then increases when the insulation thickness increases. The optimal insulation thickness and the maximum life cycle saving increase from 0.07 m to 0.17 m and from 61.2 ¥/m to 421.8 ¥/m, the payback period reduces from 9.96 year to 4.91 years respectively when the rock temperature increases from 35 ºC to 45 ºC.

This study presents a preliminary investigation on how the thermal insulation can be used to save the cooling energy and overall system cost in the mining environment in an effective and economic way. More factors, including CO_2 emission and environmental conditions, need to be accounted for in further investigations to gain an in-depth understanding on how to effectively minimise the overall energy consumption in the mining industry, thereby contributing to the carbon neutral target.

Acknowledgements

The authors thank the National Natural Science Foundation of China (51978653) and Higher Education Discipline Innovation Project (B14021) for funding this study. The authors also thank five anonymous reviewers for their constructive suggestions on this study.

Appendix:

The Eqs. (1)-(4) can be solved by using the variable-separation-method. According to the superposition principle, the solution for above equations can be expressed by Eq. (A1):

$$\begin{cases} T_1(r,t) = T_1^{(1)} + T_1^{(2)} \\ T_2(r,t) = T_2^{(1)} + T_2^{(2)} \end{cases} \tag{A1}$$

where the superscript '(1)' represents the unsteady state solution, and the superscript '(2)' represents the steady-state solution.

For the steady-state solution, the basic equations are:

$$\frac{\partial^2 T_2^{(2)}}{\partial r^2} + \frac{1}{r}\frac{\partial T_2^{(2)}}{\partial r} = 0 \tag{A2}$$

$$\frac{\partial^2 T_1^{(2)}}{\partial r^2} + \frac{1}{r}\frac{\partial T_1^{(2)}}{\partial r} = 0 \tag{A3}$$

$$T_2^{(2)}(r_3,t) = T_0 \tag{A4}$$

$$r = r_1: \quad k_1 \frac{\partial T_1^{(2)}}{\partial r} = h\left(T_1^{(2)} - T_a\right) \tag{A5a}$$

$$r = r_2: \quad \begin{cases} T_1^{(2)}\left(r_2,t\right) = T_2^{(2)}\left(r_2,t\right) \\ k_1 \dfrac{\partial T_1^{(2)}(r_2,t)}{\partial r} = k_2 \dfrac{\partial T_2^{(2)}(r_2,t)}{\partial r} \end{cases} \tag{A5b}$$

The general solutions for Eq. (A2) and Eq. (A3) are given by Eq. (A6) and Eq. (A7):

$$T_1^{(2)}(r) = C_1 \ln r + D_1 \tag{A6}$$

$$T_2^{(2)}(r) = C_2 \ln r + D_2 \tag{A7}$$

Eq. (A6) and Eq. (A7) are substituted into Eq. (A4) and Eq. (A5), the coefficients C_1, C_2, D_1, D_2 can be obtained by using Eq. (A8):

$$\begin{cases} C_1 = (T_0 - T_a)\left[\ln r_2 + \dfrac{k_1}{hr_1} - \ln r_1 - \dfrac{k_1}{k_2}(\ln r_2 - \ln r_3)\right]^{-1} \\ C_2 = \dfrac{k_1}{k_2} C_1 \\ D_1 = \dfrac{k_1}{hr_1} C_1 - (C_1 \ln r_1 - T_a) \\ D_2 = T_0 - \dfrac{k_1}{k_2} C_1 \ln r_3 \end{cases} \tag{A8}$$

For the unsteady state solution, the governing equation and the contact boundary condition are also described by Eq. (1) and Eq. (4). The initial condition and boundary condition are given by Eq. (A9) and Eq. (A10):

$$\begin{cases} T_2^{(1)}(r_3, t) = 0 \\ k_1 \dfrac{\partial T_1^{(1)}}{\partial r}\Big|_{r=r_1} = h T_1^{(1)}\Big|_{r=r_1} \end{cases} \tag{A9}$$

$$\begin{cases} T_1^{(1)}(r, 0) = T_0 - T_1^{(2)}(r) \\ T_2^{(1)}(r, 0) = T_0 - T_2^{(2)}(r) \end{cases} \tag{A10}$$

The unsteady state equation can be solved by using the separation-of-variables method [40, 43], and the following form of temperature is adopted for both insulation layer and surrounding rock regions (subscripts and superscripts are omitted):

$$T(r, t) = R(r) \cdot \Gamma(t) \tag{A11}$$

Substituting Eq. (A11) into the governing equation, two ordinary differential equations can be obtained in the form of Eq. (A12) and Eq. (A13):

$$\Gamma'(t) + \alpha \beta^2 \Gamma(t) = 0 \tag{A12}$$

$$r^2R''(r)+rR'(r)+\beta^2r^2R(r)=0 \quad \text{(A13)}$$

where β is the positive eigenvalue.

The fundamental solution of Eq. (A12) is given by Eq. (A14):

$$\Gamma(t)=\exp(-\alpha\beta^2) \quad \text{(A14)}$$

The general solution of Eq. (A13) can be expressed by Eq. (A15):

$$R(r)=A_1J_0(\beta r)+B_1Y_0(\beta r) \quad \text{(A15)}$$

Therefore, the general form of the unsteady state solution is derived and described by Eq. (A16):

$$T_i^{(1)}(r,t)=\sum_{n=1}^{\infty}\left[A_{in}J_0(\beta_{in}r)+B_{in}Y_0(\beta_{in}r)\right]\cdot\exp(-\alpha_i\beta_{in}^2t) \quad \text{(A16)}$$

The coefficients of A_{in}, B_{in}, β_{in} can be solved from the initial condition and boundary conditions and the contact boundary condition.

From the contact boundary condition, Eq. (A17) can be obtained:

$$\alpha_1\beta_{1n}^2=\alpha_2\beta_{2n}^2=\beta_n^2 \quad \text{(A17)}$$

Substituting Eq. (A17) into Eq. (A16), it is obtained as:

$$T_i^{(1)}(r,t)=\sum_{n=1}^{\infty}\left[A_{in}J_0\left(\frac{\beta_n}{\sqrt{\alpha_i}}r\right)+B_{in}Y_0\left(\frac{\beta_n}{\sqrt{\alpha_i}}r\right)\right]\cdot\exp(-\beta_n^2t) \quad \text{(A18)}$$

References:

[1] Sasmito AP, Kurnia JC, Birgersson E, Mujumdar AS. Computational evaluation of thermal management strategies in an underground mine. Appl Therm Eng. 2015;90:1144-50.

[2] Wang YJ, Zhou GQ, Wu L. Unsteady heat-moisture transfer of wet airway in deep mining. J Cent South Univ. 2013;20:1971-7.

[3] Castillo Dd. Air cycle refrigeration system for cooling deep mines. International Journal of Refrigeration. 1988;11:87-91.

[4] Chen W, Liang SQ, Liu J. Proposed split-type vapor compression refrigerator for heat hazard control in deep mines. Appl Therm Eng. 2016;105:425-35.

[5] Guo PY, He MC, Zheng LG, Zhang N. A geothermal recycling system for cooling and heating in deep mines. Appl Therm Eng. 2017;116:833-9.

[6] Walt Jvd, Kock EMd. Developments in the engineering of refrigeration installations for cooling mines. International

Journal of Refrigeration. 1984;7:27-40.
[7] Qi P, He M, Meng L, Chen C. Working principle and application of HEMS with lack of a cold source. Mining Science and Technology (China). 2011;21:433-8.
[8] du Plessis GE, Liebenberg L, Mathews EH. Case study: The effects of a variable flow energy saving strategy on a deep-mine cooling system. Appl Energ. 2013;102:700-9.
[9] Du Plessis GE, Liebenberg L, Mathews EH, Du Plessis JN. A versatile energy management system for large integrated cooling systems. Energ Convers Manage. 2013;66:312-25.
[10] Bornman W, Dirker J, Arndt DC, Meyer JP. Integrated energy simulation of a deep level mine cooling system through a combination of forward and first-principle models applied to system-side parameters. Appl Therm Eng. 2017;123:1166-80.
[11] Bahadori A, Vuthaluru HB. A simple method for the estimation of thermal insulation thickness. Appl Energ. 2010;87:613-9.
[12] Daouas N, Hassen Z, Aissia HB. Analytical periodic solution for the study of thermal performance and optimum insulation thickness of building walls in Tunisia. Appl Therm Eng. 2010;30:319-26.
[13] Ozel M. Thermal performance and optimum insulation thickness of building walls with different structure materials. Appl Therm Eng. 2011;31:3854-63.
[14] Brecani R, Dervishi S. Thermal and energy performance evaluation of underground bunkers: An adaptive reuse approach. Sustain Cities Soc. 2019;46.
[15] Wagner H. The management of heat flow in deep mines. Geomechanics and Tunnelling. 2013;4:157-63.
[16] Wang Y, Zhou G, Zhou Y. Heat transfer and environmental effects for underground engineering. Beijing: Science Press; 2019.
[17] Liu W, Apel D, Bindiganavile V, Szymanski J. Analytical and numerical modeling for the effects of thermal insulation in underground tunnels. Int J Min Sci Technol. 2016;26:267-76.
[18] Zhang Y. Transient temperature field of srrounding rock of the high geothermal roadway and its heat control mechanism by heat insulation. Xuzhou: China University of Mining and Technology; 2013.
[19] Zhu S. Research on thermal environment characteristics and heat control technology in ultra-deep mine. Taiyuan: Taiyuan University of Technology; 2017.
[20] Liu YF. Study on geopolymer foam materials and thermal insulation performance in deep roadway. Xuzhou: China University of Mining and Technology; 2018.
[21] Wu D. Experimental study on spraying insulation mechanism of high ground temperature roadway. Xuzhou: China University of Mining and Technology; 2019.
[22] Kaynakli O. A review of the economical and optimum thermal insulation thickness for building applications. Renew Sust Energ Rev. 2012;16:415-25.
[23] Kaynakli O. Economic thermal insulation thickness for pipes and ducts: A review study. Renew Sust Energ Rev. 2014;30:184-94.
[24] Ertürk M. A new approach to calculate the energy saving per unit area and emission per person in exterıor wall of building using different insulation materials and air gap. Journal of the Faculty of Engineering and Architecture of Gazi University. 2016;31:395-406.
[25] Ertürk M. A new model for exergetic optimum insulation thickness. International Journal of Exergy. 2017;22:309-30.
[26] Özel G, Açıkkalp E, Görgün B, Yamık H, Caner N. Optimum insulation thickness determination using the environmental and life cycle cost analyses based entransy approach. Sustain Energy Techn. 2015;11:87-91.
[27] Motaghian S, Monajati Saharkhiz MH, Rayegan S, Pasdarshahri H, Ahmadi P, Rosen MA. Techno-economic multi-

objective optimization of detailed external wall insulation scenarios for buildings in moderate-dry regions. Sustain Energy Techn. 2021;46:101256.

[28] Dombayci OA. The environmental impact of optimum insulation thickness for external walls of buildings. Build Environ. 2007;42:3855-9.

[29] Dlimi M, Iken O, Agounoun R, Zoubir A, Kadiri I, Sbai K. Energy performance and thickness optimization of hemp wool insulation and air cavity layers integrated in Moroccan building walls'. Sustain Prod Consump. 2019;20:273-88.

[30] Kecebas A, Alkan MA, Bayhan M. Thermo-economic analysis of pipe insulation for district heating piping systems. Appl Therm Eng. 2011;31:3929-37.

[31] Ertürk M. Optimum insulation thicknesses of pipes with respect to different insulation materials, fuels and climate zones in Turkey. Energy. 2016;113:991-1003.

[32] Daşdemir A, Ertürk M, Keçebaş A, Demircan C. Effects of air gap on insulation thickness and life cycle costs for different pipe diameters in pipeline. Energy. 2017;122:492-504.

[33] Daşdemir A, Ural T, Ertürk M, Keçebaş A. Optimal economic thickness of pipe insulation considering different pipe materials for HVAC pipe applications. Appl Therm Eng. 2017;121:242-54.

[34] Huang J, Lv H, Gao T, Feng W, Chen Y, Zhou T. Thermal properties optimization of envelope in energy-saving renovation of existing public buildings. Energ Buildings. 2014;75:504-10.

[35] Adamczyk J, Dylewski R. The impact of thermal insulation investments on sustainability in the construction sector. Renew Sust Energ Rev. 2017;80:421-9.

[36] S.P. D. Designing Green Cement Plants: Butterworth-Heinemann; 2015.

[37] Hasan A. Optimizing insulation thickness for buildings using life cycle cost. Appl Energ. 1999;63:115-24.

[38] Dombayci OA, Atalay O, Acar SG, Ulu EY, Ozturk HK. Thermoeconomic method for determination of optimum insulation thickness of external walls for the houses: Case study for Turkey. Sustain Energy Techn. 2017;22:1-8.

[39] Alsayed MF, Tayeh RA. Life cycle cost analysis for determining optimal insulation thickness in Palestinian buildings. J Build Eng. 2019;22:101-12.

[40] Wang Y, Zhou G, Wu L, Zhou Y, Lu Y. An analytical study of unsteady heat transfer in the rock surrounding a deep airway. International Journal of Mining Science and Technology. 2012;22:411-5.

[41] Kang FC, Li YC, Tang CA. Numerical study on airflow temperature field in a high-temperature tunnel with insulation layer. Appl Therm Eng. 2020;179.

[42] Bergman TL, Lavine AS. Fundamentals of Heat and Mass Transfer: John Wiley & Sons; 2017.

[43] Hahn DW, Ozisik MN. Heat Conduction. New York: John Wiley & Sons; 2012.

[44] Basbagill J, Flager F, Lepech M, Fischer M. Application of life-cycle assessment to early stage building design for reduced embodied environmental impacts. Build Environ. 2013;60:81-92.

[45] Wang Y, Zheng T, Zheng X, Liu Y, Darkwa J, Zhou G. Thermo-mechanical and moisture absorption properties of fly ash-based lightweight geopolymer concrete reinforced by polypropylene fibers. Constr Build Mater. 2020;251:118960.

[46] Schlichting H, Gersten K. Boundary-Layer Theory: Springer; 2017.

[47] Starfield A, Bleloch A. A new method for the computation of heat and moisture transfer in a partly wet airway. J South Afr Inst Min Metall. 1983;83:263-9.

[48] Wang Y, Zhou G, Wei Y, Kuang L, Wu L. Experimental research on changes in the unsteady temperature field of an airway in deep mining engineering. J China Univ Min Technol. 2011;40:345-50.

[49] Wang H, Zhou QY. Finite Element Analysis of Surrounding Rock with a Thermal Insulation Layer in a Deep Mine. Math Probl Eng. 2020;2020.

[50] Wang JH, Wan ZJ, Zhang HW, Wu D, Zhang Y, Wang Y, et al. Application of Thermal Insulation Gunite Material to the High Geo-Temperature Roadway. Advances in Civil Engineering. 2020;2020.

[51] Zhou XH, Tang XY, Song DP. Thermal insulation performance affected by thermal physical parameters of thermal insulation layer in active thermal insulation tunnel. Mining Safety and Environmental Protection. 2019;46:14-8.
[52] Yuan Z, Zhijun W, Zhaoyang M, Bin G, Yangsheng M. Heat transfer analysis of surrounding rocks with thermal insulation layer in high geothermal roadway. Thermal Science. 2019;23:777-90.
[53] Idchabani R, Khyad A, Ganaoui ME. Optimizing insulation thickness of external walls in cold region of Morocco based on life cycle cost analysis. Energy Procedia. 2017;139:117-21.